Divertor power load studies in ASDEX Upgrade and TCV

M.Faitsch[1], S.Coda[2], T.Eich[1], A.Gallo[3], B.Labit[2], R.Maurizio[2], A.Merle[2],
H.Reimerdes[2], B.Sieglin[1], W.Suttrop[1], C.Theiler[2], H.Zohm[1],
the ASDEX Upgrade*, TCV† and EUROfusion MST1‡ teams

[1] *Max-Planck-Institute for Plasma Physics, Boltzmannstr. 2, 85748 Garching, Germany*

[2] *Ecole Polytechnique Federale de Lausanne, Swiss Plasma Center, 1015 Lausanne, Switzerland*

[3] *Aix Marseille Univ, CNRS, PIIM, UMR 7345, Marseille 13397, France*

Introduction

In recent years the focus of tokamak fusion research onto power exhaust increased showing that first wall power load is one of the major challenges in realizing a power plant [1, 2]. Unmitigated divertor power loads in next step fusion devices like ITER are projected to exceed material limits making significant impurity seeding necessary. Furthermore, scenarios without large type-I edge localized modes (ELMs) are desired for a future reactor. Two possible regimes, among others, are the operation with negative triangularity L-mode and type-I ELM suppressed or mitigated H-mode using an external magnetic perturbation (MP) field. However, steady state power exhaust under these conditions is an open field of research. Shaping the plasma to negative triangularity was pioneered at TCV showing in L-mode, a natural ELM free regime, improved core confinement compared to positive triangularity [3, 4]. ELM suppression and mitigation by an external MP field is studied in most of today's tokamaks.

Effect of varying upper triangularity on divertor power load in TCV

Shaping the plasma boundary can change the power fall-off length, measured at the outer divertor target λ_q^{out}, beyond established empirical multi machine scaling laws typically using global plasma parameters without dedicated shaping scans [5]. This section summarizes the results presented in [6]. Changing the upper triangularity leads to changes in confinement as well as the λ_q in the presented TCV L-mode data set. The correlation between λ_q^{out} and the upper triangularity δ_{up} is shown in figure 1 (left) and the correlation with the edge electron temperature $T_{e,edge}$ is shown in figure 1 (right). Extending an L-mode scaling law from ASDEX Upgrade [7] reveals a dependence on edge electron temperature $T_{e,edge}$ in both machines and no explicit size dependence. Enhanced energy confinement at negative triangularity, explained by a reduction of turbulent transport in the confined region [8], is confirmed. The effect of triangularity on scrape-off layer turbulence could be a possible explanation for smaller λ_q^{out} for decreasing δ_{up}, in qualitative agreement with turbulence simulation in limited plasmas [9].

*See author list of "MEYER, H. et al, Nucl. Fusion accepted (2019) (https://doi.org/10.1088/1741-4326/ab18b8)"
†See author list of "CODA, S. et al, Nucl. Fusion accepted (2019) (https://doi.org/10.1088/1741-4326/ab25cb)"
‡See author list of "LABIT, B. et al, Nucl. Fusion **59** (2019) 086020."

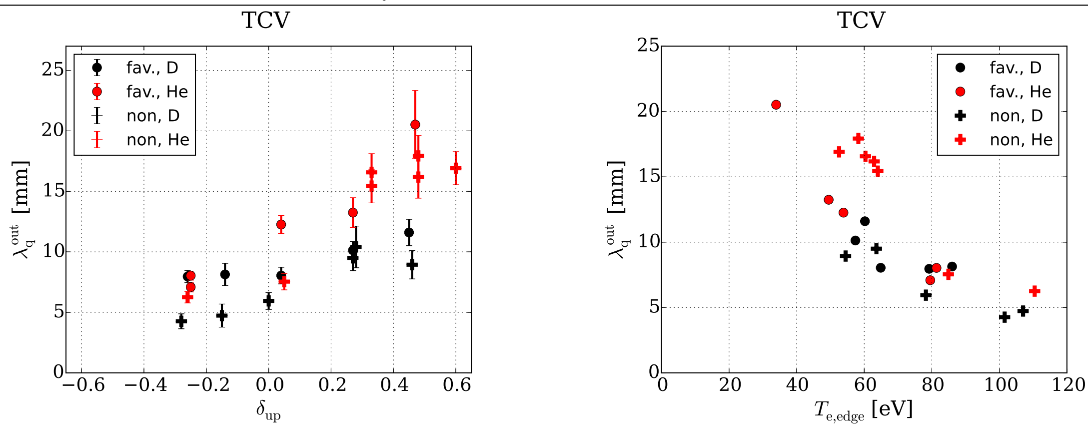

Figure 1: Correlation between power fall-off length measured at the outer divertor target λ_q^{out} and (left) upper triangularity δ_{up} and (right) edge electron temperature $T_{e,edge}$ for deuterium (D) and helium (He) plasmas with ion ∇B drift towards the active X-point (fav.) and away from it (non).

Helium discharges exhibit a larger λ_q^{out} compared to deuterium, in line with previous studies on JET [10] and ASDEX Upgrade [11]. Reversal of the vertical drift direction has no significant influence on both, λ_q^{out} and λ_q^{in}, in the presented data set. The power fall-off length measured at the inner divertor target exhibits a non monotonic behaviour for changing δ_{up}. The largest λ_q^{in} is obtained for $\delta_{up} \approx 0$. The asymmetry between inner and outer λ_q is compared to an interpretation [11] of the heuristic drift-based model [12], finding partial agreement at positive, and no agreement at negative δ_{up}. The similarity between observations comparing both vertical drift directions challenge the assumption of a drift-based transport.

Considerations of a negative triangularity reactor due to reduced core turbulence and larger major radius of the divertor R_{div} apply λ_q from scaling laws deduced from positive triangularity discharges. The effect of a smaller λ_q for negative δ needs to be taken into account for an overall assessment of such novel configurations in order to assess the expected divertor power load.

Effect of external magnetic perturbation on divertor power load in ASDEX Upgrade

Applying an external magnetic perturbation leads to a major change in the divertor heat flux pattern. This section summarizes results from [13, 14, 15]. The inter-ELM and L-mode pattern, being axisymmetric without MP, develop a 2D structure. This structure is reproduced for the investigated discharges in both L- and H-mode with a simplified scrape-off layer model, see [14], based on field line tracing.

The 2D divertor target heat flux profile is shown in figure 2 for both experimental measurement (left) and modeling (right) of an ASDEX Upgrade L-mode discharge with a *resonant* MP, where the MP is field line aligned at the plasma edge. A 1D heat flux profile is extracted for a certain toroidal angle and the comparison between experimental profile and modeled profile is shown in figure 3. The comparison shows not only excellent agreement in the 2D structure of the heat load but also on the absolute and relative height of the local maxima and minima. A deviation is

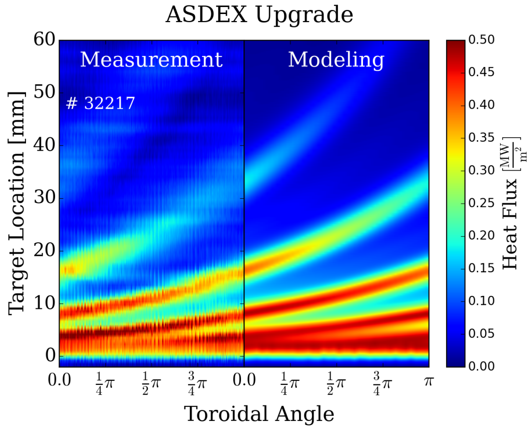

Figure 2: 2D heat flux profiles obtained by IR measurements (left) and modeling (right) for # 32217 with a *resonant* external MP.

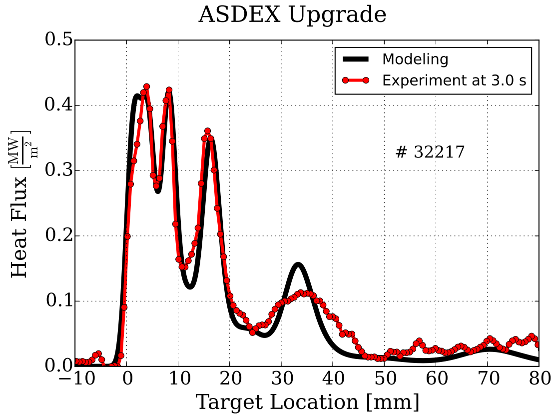

Figure 3: 1D heat flux profiles obtained by IR measurements (red) and modeling (black) for # 32217 with a *resonant* external MP.

observed far from the peak heat flux, attributed to a stronger broadening in this region compared to the location close to the strike line, whereas the model assumes a uniform broadening.

The toroidally averaged experimental heat flux profile in L-mode with MP is similar to the reference profile without MP, being characterized by the same values for the transport qualifiers, power fall-off length λ_q and divertor broadening S. No change in the heat transport is observed, in line with the model prediction. The peak heat flux is unchanged for all toroidal phases with rotating MP. This is the same location as in the reference phase without MP.

Although the toroidally averaged heat flux is unchanged, the application of the MP has an effect onto the toroidal variation of the heat flux away from the peak. The toroidal variation for a given MP and plasma configuration is quantified by a newly introduced parameter called *toroidal peaking*. The peaking is defined as the toroidal maximum normalized to the averaged value and is largest for the *resonant* MP configuration and at lowest density with up to a factor of about 2 at the position one power fall-off length away from the strike line. The variation decreases by shifting the alignment away from the *resonant* configuration. For the *non-resonant* configuration no changes are observed outside typical heat flux variations in L-mode.

A density increase leads to a reduced *toroidal peaking* and a nearly axisymmetric profile in attached divertor conditions for the discharge parameters obtained in the discussed L-mode study. The local decrease of the plasma temperature in the divertor caused by the increased density increases the divertor broadening S for the outer divertor of ASDEX Upgrade [7]. The reduction of the *toroidal peaking* is explained by the model through the increase of the divertor broadening S solely and is in quantitative agreement with the measurements.

The comparison of the model with experimental data suggests a linear increase of the *toroidal peaking* with MP coil current, i.e. perturbation strength. Increasing the fundamental mode number of the external MP reduces the *toroidal peaking*.

Previous studies reported that in H-mode the peak heat load caused by ELMs correlates with the pedestal top pressure [16]. This correlation is confirmed in presence of a MP field [15]. However, ELM filaments, that, without MP, are expelled at varying toroidal positions, are *locking* to the external MP field, leading to enhanced sputtering and thermal loads on distinguished toroidal locations with respect to the phase of the MP.

In a certain regime, mainly at low density and rotation, an external MP can penetrate the plasma and lead to magnetic reconnection generating magnetic islands at resonant flux surfaces. This is observed in low density L-mode discharges with a $n = 1$ MP leading to a fundamentally different heat flux pattern at the divertor target. The heat flux structure is in line with connection length L_c calculations due to an ergodization of field lines at the plasma boundary with neighbouring field lines having significant different L_c. However, the extent along the target location is considerably larger than in discharges without field penetration and cannot be explained by the vacuum field of the external MP. Due to the field penetration a flattening of the temperature profile around the $q = 2$ flux surface is observed, interpreted as a magnetic island. Characterizing this island as a current perturbation leads to similar L_c patterns as observed with an external MP. The observed heat flux pattern is in line with an ergodization of the plasma edge due to the superposition of the external MP and the internal magnetic island being locked in phase.

Acknowledgements

This work has been carried out within the framework of the EUROfusion Consortium and has received funding from the Euratom research and training programme 2014-2018 and 2019-2020 under grant agreement No 633053. The views and opinions expressed herein do not necessarily reflect those of the European Commission.

References

[1] LOARTE, A. et al, Nucl. Fusion **47** (2007) S203.
[2] PITTS, R. et al, J. Nucl. Mater. **438** (2013) S48.
[3] MORET, J.-M. et al, Phys. Rev. Lett. **79** (1997) 2057.
[4] POCHELON, A. et al, Nucl. Fusion **39** (1999) 1807.
[5] EICH, T. et al, Nucl. Fusion **53** (2013) 093031.
[6] FAITSCH, M. et al, Plasma Phys. Control. Fusion **60** (2018) 045010.
[7] SIEGLIN, B. et al, Plasma Phys. Control. Fusion **58** (2016) 055015.
[8] MARINONI, A. et al, Plasma Phys. Control. Fusion **51** (2009) 055016.
[9] RIVA, F. et al, Plasma Phys. Control. Fusion **59** (2017) 035001.
[10] PITTS, R. A. et al, J. Nucl. Mater. **337-339** (2005) 146.
[11] FAITSCH, M. et al, Plasma Phys. Control. Fusion **57** (2015) 075005.
[12] GOLDSTON, R. J., Nucl. Fusion **52** (2012) 013009.
[13] FAITSCH, M. et al, Nucl. Mater. Energy **12** (2017) 1020.
[14] FAITSCH, M. et al, Plasma Phys. Control. Fusion **59** (2017) 095006.
[15] FAITSCH, M. et al, Plasma Phys. Control. Fusion **61** (2019) 014008.
[16] EICH, T. et al, Nucl. Mater. Energy **12** (2017) 84.